DEUTSCHES ELEKTRONEN-SYNCHROTRON

DESY 94-111
July 1994

Measurement of the Decay Fractions of D^* Mesons

The ARGUS Collaboration

ISSN 0418-9833

NOTKESTRASSE 85 - 22603 HAMBURG

To be sure that your preprints are promptly included in the
HIGH ENERGY PHYSICS INDEX,
send them to (if possible by air mail):

DESY **Bibliothek** **Notkestraße 85** **22603 Hamburg** **Germany**	**DESY-IfH** **Bibliothek** **Platanenallee 6** **15738 Zeuthen** **Germany**

DESY 94-111
July 1994

ISSN 0418-9833

Measurement of the Decay Fractions of D^* Mesons

The ARGUS Collaboration

H. Albrecht, H. Ehrlichmann, T. Hamacher, R. P. Hofmann, T. Kirchhoff, R. Mankel[1], A. Nau, S. Nowak[1], D. Reßing, H. Schröder, H. D. Schulz, M. Walter[1], R. Wurth
DESY, Hamburg, Germany

C. Hast, H. Kapitza, H. Kolanoski, A. Kosche, A. Lange, A. Lindner, M. Schieber, T. Siegmund, B. Spaan, H. Thurn, D. Töpfer, D. Wegener
Institut für Physik[2], Universität Dortmund, Germany

P. Eckstein, M. Schmidtler, M. Schramm, K. R. Schubert, R. Schwierz, R. Waldi
Institut für Kern- und Teilchenphysik[3], Technische Universität Dresden, Germany

M. Paulini, K. Reim, H. Wegener
Physikalisches Institut[4], Universität Erlangen-Nürnberg, Germany

R. Eckmann, H. Kuipers, O. Mai, R. Mundt, T. Oest, R. Reiner, W. Schmidt-Parzefall
II. Institut für Experimentalphysik, Universität Hamburg, Germany

J. Stiewe, S. Werner
Institut für Hochenergiephysik[5], Universität Heidelberg, Germany

K. Ehret, W. Hofmann, A. Hüpper, S. Khan, K. T. Knöpfle, J. Spengler
Max-Planck-Institut für Kernphysik, Heidelberg, Germany

P. Krieger[6], D. B. MacFarlane[7], J. D. Prentice[6], P. R. B. Saull[7], K. Tzamariudaki[7], R. G. Van de Water[6], T.-S. Yoon[6]
Institute of Particle Physics[8], Canada

C. Frankl, C. Ratz, M. Schneider, S. Weseler
Institut für Experimentelle Kernphysik[9], Universität Karlsruhe, Germany

G. Kernel, P. Križan, E. Križnič, T. Podobnik, T. Živko
Institut J. Stefan and Oddelek za fiziko[10], Univerza v Ljubljani, Ljubljana, Slovenia

V. Balagura, I. Belyaev, V. Blinov[11], S. Chechelnitsky, M. Danilov, A. Droutskoy, Yu. Gershtein, A. Golutvin, I. Korolko, G. Kostina, D. Litvintsev, V. Lubimov, P. Pakhlov, S. Semenov, A. Snizhko, I. Tichomirov, A. Undrus[11], Yu. Zaitsev, V. Zhilich[11]
Institute of Theoretical and Experimental Physics, Moscow, Russia

[1] DESY, IfH Zeuthen

[2] Supported by the German Bundesministerium für Forschung und Technologie, under contract number 054DO51P.
[3] Supported by the German Bundesministerium für Forschung und Technologie, under contract number 056DD11P.
[4] Supported by the German Bundesministerium für Forschung und Technologie, under contract number 054ER12P
[5] Supported by the German Bundesministerium für Forschung und Technologie, under contract number 055HD21P.
[6] University of Toronto, Toronto, Ontario, Canada.
[7] McGill University, Montreal, Quebec, Canada.
[8] Supported by the Natural Sciences and Engineering Research Council, Canada.
[9] Supported by the German Bundesministerium für Forschung und Technologie, under contract number 055KA11P.
[10] Supported by the Ministry of Science and Technology of the Republic of Slovenia and the Internationales Büro KfA, Jülich.
[11] on leave of absence from the Institute of Nuclear Physics, Novosibirsk, Russia

Abstract

Using the ARGUS detector at the DORIS II electron-positron storage ring at DESY, we have measured $\mathrm{BR}(D^{*+} \to D^0\pi^+) = (68.8 \pm 3.6 \pm 1.9)\%$, $\mathrm{BR}(D^{*+} \to D^+\pi^0) = (31.2 \pm 1.6 \pm 1.0)\%$, $\mathrm{BR}(D^{*+} \to D^+\gamma) < 5.2\%$ (90%CL), $\mathrm{BR}(D^{*0} \to D^0\pi^0) = (59.6 \pm 3.5 \pm 2.8)\%$, and $\mathrm{BR}(D^{*0} \to D^0\gamma) = (40.4 \pm 3.5 \pm 2.8)\%$, and the mass difference $\Delta m_0 = m(D^{*0}) - m(D^0) = (142.2 \pm 0.3 \pm 0.2)\mathrm{MeV}/c^2$.

The vector mesons D^{*+} and D^{*0} may decay via strong interaction to $D\pi$ final states, or via electromagnetic transitions to $D\gamma$. The latter are proportional to the magnetic moment of the constituent quarks [1], which allows an important test of the Standard Model for the heavy quark c. All decays have been measured previously [2–7]. The world average [8] of $\mathrm{BR}(D^{*+} \to D^+\gamma) = (18 \pm 4)\%$, which is mainly due to a single measurement [7], can only be explained by non-standard models, e.g. assuming a large anomalous magnetic moment of the charm quark [9]. A recent measurement by CLEO [10] gives a much lower result, $\mathrm{BR}(D^{*+} \to D^+\gamma) = (1.1 \pm 1.4 \pm 1.6)\%$, which is in good agreement with the Standard Model. In addition, the CLEO value for $\mathrm{BR}(D^{*0} \to D^0\gamma)$ is smaller than any previous result, although it is statistically compatible. These facts call for further independent measurements. A clarification is also desirable because D^* branching fractions have a noticeable impact on the measurements of the branching fractions of B meson decays.

The analyses reported here are based on data taken with the ARGUS detector [11] in the energy region around $\sqrt{s} = 10\,\mathrm{GeV}$ on the Υ resonances and in the nearby continuum, together comprising an integrated luminosity of 476/pb.

D^{*0} reconstruction

Charged particles are required to originate from the main vertex with a polar angle θ in the range $|\cos\theta| < 0.92$. Particles are identified by combining available information from several detector components into a likelihood [11] for each of the hypotheses e, μ, π, K, and p, which is accepted if the normalized likelihood exceeds 0.01.

In events with at least three charged tracks from the interaction region, D^0 meson[1] candidates are selected in the decay modes $K^-\pi^+$ and $K^-\pi^+\pi^+\pi^-$. The $K^-\pi^+$, $(K^-\pi^+\pi^+\pi^-)$ combinations with a mass within $\pm 30\,(20)\,\mathrm{MeV}/c^2$ of the nominal mass are kinematically constrained to the proper value [8]. To avoid double counting, which occurs mainly when a K changes role with a π, only one combination for each D^0 decay mode per event was allowed by selecting the candidate with the maximum χ^2-probability of this fit.

Combinatoric background from the copious soft pions in multihadron events can be reduced, if we avoid combinations where the kaon is in the very forward direction.

[1] References in this paper to a specific charged state also imply the charged conjugate state.

Therefore, we require $\cos\theta^*_K < 0.8$, where θ^*_K is the direction of flight of the kaon in the centre of mass system of the D candidate with respect to its boost direction.

Energy clusters in the calorimeter are considered as photons if they exceed 80 MeV and are not associated with a charged track. For π^0 reconstruction we use photons from the total solid angle covered by the calorimeter, $|\cos\theta_\gamma| < 0.92$. Photon pairs with an invariant mass within $\pm 50\,\mathrm{MeV}/c^2$ of the nominal π^0 mass are accepted and kinematically constrained to its value.

D^0 candidates are combined with these reconstructed π^0 mesons and with photons from the barrel region of the calorimeter, $|\cos\theta_\gamma| < 0.70$, and with energy larger than 100 MeV. The higher energy cut reduces the background originating from noise in the shower counters.

Since the D^* momentum spectrum peaks at high momenta while the combinatoric background peaks at low momenta, we required $x_p > 0.6$ for D^{*0} candidates, where $x_p = p/\sqrt{E^2_{beam} - m^2}$ is the scaled momentum.

There is a large background in both modes due to random combinations of D^0 mesons with soft photons or pions, which can be substantially suppressed by the requirement $\cos\theta^*_{\gamma/\pi^0} > -0.8$, where θ^*_{γ/π^0} is the angle of the γ or π^0 in the D^0 rest frame with respect to the boost direction.

In the $D^{*0} \to D^0\gamma$ mode a large combinatoric background arises from photons produced by π^0 decays. To reduce this background to a manageable level, the following additional requirements are applied:

combinatorics cut: No more than 6 photons with $E_\gamma > 80\,\mathrm{MeV}$ are allowed in the event.

This requirement has an efficiency for the $D^{*0} \to D^0\gamma$ signal of 68%, while the background was suppressed by a factor of 3.

anti-π^0 cut: Combinations are rejected if the photon combined with any other photon in the event has an invariant mass within $\pm 50\,\mathrm{MeV}/c^2$ of the nominal π^0 mass.

The efficiency of this requirement is determined to be 63% for the $D^{*0} \to D^0\gamma$ signal, while the background was further suppressed by a factor of 4.

After application of these cuts, the $D^0\gamma$ and $D^0\pi^0$ mass distributions show prominent peaks near the D^{*0} mass, while there is no signal in the D^0 sideband regions. A major fraction of the background in the invariant mass distributions can be attributed to combinatoric background under the D^0 peak. We subtracted the $(K^-\pi^+, K^-\pi^+\pi^+\pi^-)\gamma$ and $(K^-\pi^+, K^-\pi^+\pi^+\pi^-)\pi^0$ mass spectra, using $K^-\pi^+$ and $K^-\pi^+\pi^+\pi^-$ combinations from the sidebands normalized to the number of background events under the signal.

The resulting distributions for $D^0\gamma$ are shown in figure 1. The peak at low mass values is a feeddown from the decay $D^{*0} \to D^0\pi^0 \to D^0\gamma(\gamma)$. If only one of the photons from the π^0 is used to make an entry in the mass distribution, the corresponding D^*

Table 1 Summary of the determination of the decay ratio $R_0 = \mathrm{BR}(D^{*0} \to D^0\gamma)/\mathrm{BR}(D^{*0} \to D^0\pi^0)$.

photons	D^0 decay mode	$N(D^0\gamma)$	$N(D^0\pi^0)$	$\varepsilon_\gamma/\varepsilon_{\pi^0}$	R_0
shower, γ	$K^-\pi^+$	$202 \pm 41 \pm 36$	$245 \pm 24 \pm 20$	0.89	$0.73 \pm 0.18 \pm 0.16$
shower, π^0	$K^-\pi^+$		$165 \pm 34 \pm 35$	0.38	$0.46 \pm 0.27 \pm 0.24$
shower, γ	$K^-\pi^+\pi^+\pi^-$	$254 \pm 73 \pm 42$	$225 \pm 37 \pm 24$	0.78	$0.88 \pm 0.36 \pm 0.21$
shower, π^0	$K^-\pi^+\pi^+\pi^-$		$223 \pm 60 \pm 45$	0.36	$0.42 \pm 0.35 \pm 0.22$
converted, γ_c	both	$37.3 \pm 6.5 \pm 3$	$82.1 \pm 15 \pm 14$	1.22	$0.55 \pm 0.14 \pm 0.10$
converted, π^0	both		$25.2 \pm 6.2 \pm 3$	0.41	$0.61 \pm 0.31 \pm 0.14$
average					$0.68 \pm 0.10 \pm 0.08$

signal is shifted to lower masses. Typically, pions produced in the decay $D^* \to D\pi^0$ have very small momenta, and decays into this channel often result in one photon with an energy below 80 MeV, thus failing the anti-π^0 cut. Therefore the feeddown peak provides a very good indirect measurement of $\mathrm{BR}(D^{*0} \to D^0\pi^0)$.

The remaining background under the D^* signal is due to combinations of real D^0 mesons with random photons. The shape of this background was studied using a clean D^0 sample tagged by $D^{*+} \to D^0\pi^+$ decays together with photons from the same event.

The $D^0\gamma$ invariant mass distribution was fitted by two Gaussians corresponding to the contributions from the $D^0\gamma$ ($\sigma = 22\,\mathrm{MeV}/c^2$) and $D^0\pi^0$ ($\sigma = 15\,\mathrm{MeV}/c^2$) decay modes. The widths are determined from a Monte Carlo simulation, where we generate events with the Lund jet fragmentation program [12], which are subsequently passed through a simulation of the ARGUS detector and the event reconstruction. The background shape is fixed from the study described above. The solid curve in figure 1 shows the result of the fit and the dotted line represents the background shape. From this fit, we obtain the numbers listed as "shower, γ" results in table 1. Systematic errors in addition to the uncertainty in the efficiencies are determined by varying the fit parameters and background shape within their errors.

The $D^0\pi^0$ invariant mass distributions after D^0 sideband subtraction for $D^0 \to K^-\pi^+$ and $D^0 \to K^-\pi^+\pi^+\pi^-$ are shown in figure 2. There are prominent D^{*0} peaks in both cases. The spectra are fitted with a parametrization of the signal peak as the sum of two Gaussians and a background with a shape fixed from the D^{*+} study. The widths of the Gaussians are fixed to 3.0 and 6.0 MeV/c^2 as determined from the Monte Carlo simulation: the tails described by the wider part are mainly due to overlapping shower clusters in the electromagnetic calorimeter. The solid curve in figure 2 represents the best fit and the dotted line shows the background behaviour. The resulting numbers of events for the $D^0\pi^0$ signal are also given in table 1.

The ratio of branching fractions

$$R_0 = \frac{\mathrm{BR}(D^{*0} \to D^0\gamma)}{\mathrm{BR}(D^{*0} \to D^0\pi^0)} = \frac{N(D^{*0} \to D^0\gamma)}{\varepsilon(D^{*0} \to D^0\pi^0)} \frac{\varepsilon(D^{*0} \to D^0\gamma)}{N(D^{*0} \to D^0\pi^0)}$$

has been calculated for all channels combining the $D^0\gamma$ average with the result from the feeddown peak, and with the result from the $D^0\pi^0$ signal. The efficiencies of the D^0 reconstruction and of the x_p cut cancel in this ratio. The geometric acceptance for the photon and the efficiency of the cut on $\cos\theta_{\gamma,\pi^0}$ are obtained from the Monte Carlo simulation. The efficiency of the combinatorics cut is extracted from data using the clean sample of D^0 mesons from the $D^{*+} \to D^0\pi^+$ decay, as the fraction of events in the D^{*+} peak surviving this cut. This is justified, since the same neutral multiplicity is expected in the events with D^{*+} as in events with D^{*0}, once the photon from the D^{*0} decay is subtracted. We obtain an efficiency of $(68 \pm 3)\%$.

The anti-π^0 cut efficiency is determined calculating the probability, that a random photon with appropriate momentum from the Monte Carlo generator combined with other photons from the data event does not have a pair mass within $\pm 50\,\mathrm{MeV}/c^2$ of the nominal π^0 mass. We obtained an anti-π^0 cut efficiency of $(63 \pm 4 \pm 2)\%$.

These two efficiencies are also reproduced by our Monte Carlo simulation within statistical errors.

D^{*0} reconstruction with converted photons

The mass resolution is enormously improved if we combine D meson candidates with converted photons $\gamma_c \to e^+e^-$, which are reconstructed in the drift chamber, compared to photons measured in the calorimeter. This is obtained at the price of an efficiency reduction by about a factor of 30.

The reconstruction of converted photons proceeds by finding a secondary vertex formed by an e^+e^- pair with invariant mass smaller than $70\,\mathrm{MeV}/c^2$ and energy greater than 80 MeV. In order to increase the statistics, we relax some cuts: Photons for π^0 reconstruction are accepted at an energy $E > 50\,\mathrm{MeV}$, the interval for the $K^-\pi^+(K^-\pi^+\pi^+\pi^-)$ mass is increased to $\pm 40(30)\,\mathrm{MeV}/c^2$, and the cuts on $\cos\theta_{\gamma,\pi^0}$, the combinatorics cut and the anti-π^0 cut are not applied.

Figure 3 shows the $D^0\gamma_c$ mass distribution. Due to the limited number of events, we have added both D^0 decay channels. A fit with signal widths fixed from the Monte Carlo simulation to $1.8\,\mathrm{MeV}/c^2$ for the D^{*0} peak and $14.6\,\mathrm{MeV}/c^2$ for the feeddown peak is applied (solid curve). The dashed line shows the background function. Figure 4 shows the $D^0\pi^0$ mass distribution, with $\pi^0 \to \gamma_c\gamma$, which is fitted using a signal width of $0.8\,\mathrm{MeV}/c$. The fit results are listed in table 1, which summarizes all measurements.

D^{*0} branching fractions

Since there are only two allowed decay modes for the D^{*0} meson, we use the constraint that the sum is unity to determine the branching fractions. From our average

Table 2 Results on $\mathrm{BR}(D^{*0} \to \gamma D^0) = 1 - \mathrm{BR}(D^{*0} \to \pi^0 D^0)$.

experiment	BR [%]
Mark I 77 [2]	45 ± 15
Mark II 82 [3]	47 ± 12
JADE 85 [4]	$53 \pm 9 \pm 10$
HRS 87 [5]	47 ± 23
Mark III 88 [7]	$37 \pm 8 \pm 8$
CLEO 92 [10]	$36.4 \pm 2.3 \pm 3.3$
this experiment	$40.4 \pm 3.5 \pm 2.8$
world average	39.5 ± 2.7

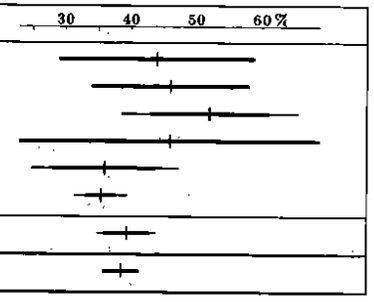

result

$$R_0 = \frac{\mathrm{BR}(D^{*0} \to D^0\gamma)}{\mathrm{BR}(D^{*0} \to D^0\pi^0)} = 0.68 \pm 0.10 \pm 0.08$$

both branching fractions can be calculated to be

$$\mathrm{BR}(D^{*0} \to D^0\gamma) = (40.4 \pm 3.5 \pm 2.8)\%$$
$$\mathrm{BR}(D^{*0} \to D^0\pi^0) = (59.6 \pm 3.5 \pm 2.8)\%$$

This result is compared with other experiments in table 2. The average of all results in this table is $\mathrm{BR}(D^{*0} \to D^0\gamma) = (39.5 \pm 2.7)\%$.

$D^{*0} - D^0$ mass difference

Exploiting the excellent momentum resolution of the converted photons, we use our D^{*0} signals for a determination of the $D^{*0} - D^0$ mass difference. The distribution of the mass difference is shown in figure 5. It is fitted with a Gaussian signal shape, including a radiative tail to account for bremsstrahlung as obtained from the Monte Carlo simulation, above a linear background. The fit yields a mass difference of $\Delta m_0 = m(D^{*0}) - m(D^0) = (142.2 \pm 0.3)\,\mathrm{MeV}/c^2$. The momentum calibration for converted photons was checked using the π^0 decay. The π^0 peak appears at $(135.2 \pm 0.3)\,\mathrm{MeV}/c^2$, consistent with the accepted value [8]. From this agreement, we deduce a systematic uncertainty of $\pm 0.2\,\mathrm{MeV}/c^2$.

This result of

$$\Delta m_0 = m(D^{*0}) - m(D^0) = (142.2 \pm 0.3 \pm 0.2)\,\mathrm{MeV}/c^2$$

is consistent with the Particle Data Group average of $(142.5 \pm 1.3)\,\mathrm{MeV}/c^2$, with a significant increase in precision. It agrees also with a recent precise measurement by the CLEO collaboration of $(142.12 \pm 0.05 \pm 0.05)\,\mathrm{MeV}/c^2$ [13].

D^{*+} reconstruction

D^+ meson candidates are selected in the channel $K^-\pi^+\pi^+$. Figure 6 shows the invariant mass distribution of these candidates: all combinations with a mass within $\pm 25\,\mathrm{MeV}/c^2$ of the nominal D^+ mass are chosen. Instead of constraining this reconstructed mass, we use the mass difference to search for $D^+\gamma$ and $D^+\pi^0$ signals. The D^+ channel has negligible double counting due to the charge combination $K^-\pi^+\pi^+$.

Combinatoric background is efficiently reduced by the requirement, that the three D^+ decay products are in the same hemisphere in the laboratory frame.

Photons with an energy larger than 100 MeV and π^0 candidates are selected in the same way as for the D^{*0} analysis and are combined with the D^+ candidates. To enhance the high-momentum D^{*+} mesons over combinatoric background, we apply a cut $x_p > 0.65$.

Background from random $K\pi\pi$ combinations is subtracted using the D^+ sidebands, which are chosen symmetric with respect to the D^+ mass as shown in figure 6. Background from D^+ combinations with random photons are described by data from D^0 tagged by $D^{*+} \to D^0\pi^+$, as described above.

After subtraction of combinatoric background, we obtain the distribution of the mass difference for $D^+\gamma$ shown in figure 7. In figure 8 the mass difference for $D^+\pi^0$ is shown together with the predicted background. Only the channel $D^{*+} \to D^+\pi^0$ is evident in both figures, while the fraction of $D^{*+} \to D^+\gamma$ is compatible with zero.

An additional source of background has to be considered for the latter channel: If a D_s from $D_s^* \to D_s\gamma$ decays to $K^-K^+\pi^+$, and the K^+ is misidentified as π^+, the resulting mass distribution shows a wide bump close to the $D^+ \to K^-\pi^+\pi^+$ peak, as shown in figure 6. The shape of this reflection has been determined by the Monte Carlo simulation, and the height is obtained from a fit of this shape, a D^+ peak and a linear background function. About 75% of these D_s mesons are from a D_s^* decay, and leave a fake signal at the mass difference $m(D^{*+}) - m(D^+) \approx m(D_s^*) - m(D_s)$.

A fit to the mass difference distribution in figure 7 using Monte Carlo distributions for $D^{*+} \to D^+\pi^0$ and $D^{*+} \to D^+\gamma$ gives the results listed in table 3. Here, the contribution of the $D_s\gamma$ combinations, which are left after the sideband subtraction, are already subtracted from the $D^+\gamma$ signal.

D^{*+} reconstruction with converted photons

We have also performed an analysis using converted photons, as described above. $K\pi\pi$ candidates within $\pm 34\,\mathrm{MeV}/c^2$ are selected, submitted to a D^+ mass constraint fit, and combined with single converted photons or $\pi^0 \to \gamma_c\gamma$.

Figure 9 shows the $D^+\gamma_c$ mass distribution, using an anti-π^0 cut of $\pm 30\,\mathrm{MeV}/c^2$ around the π^0 mass of all $\gamma_c\gamma$ combinations. A fit with signal widths fixed from the Monte Carlo simulation to $2.5\,\mathrm{MeV}/c^2$ for the D^{*+} peak and $14.6\,\mathrm{MeV}/c^2$ for the feeddown peak

Table 3 Summary of D^{*+} decay channels. The average given for the ratio R_+ corresponds to < 0.16 at 90%CL.

photons	x_p	$N(D^+\gamma)$	$N(D^+\pi^0)$	$\varepsilon_\gamma/\varepsilon_{\pi^0}$	ratio R_+
shower γ	> 0.65	-37 ± 141	1130 ± 113	0.75 ± 0.05	$-0.04 \pm 0.17 \pm 0.08$
shower π^0	> 0.65		250 ± 31	3.1 ± 0.2	$-0.03 \pm 0.18 \pm 0.09$
converted	> 0.60	0.0 ± 3.2	24.3 ± 6.1	0.96 ± 0.16	$0.00 \pm 0.14 \pm 0.05$
average					$-0.02 \pm 0.09 \pm 0.05$

is applied (solid curve). The dotted line is the signal corresponding to our 90%CL upper limit. Figure 10 shows the $D^0\pi^0$ mass distribution, with $\pi^0 \to \gamma_c\gamma$, and is fitted using a signal width of $0.8\,\mathrm{MeV}/c$.

The fit results are listed in table 3, which summarizes all measurements. We neglect here the D_s^* background, which would shift the best fit result of 0.00 only slightly into the unphysical negative regime, while the errors remain unchanged.

D^{*+} branching fractions

The ratio of branching fractions

$$R_+ = \frac{\mathrm{BR}(D^{*+} \to D^+\gamma)}{\mathrm{BR}(D^{*+} \to D^+\pi^0)}$$

has been extracted using both the results on $\mathrm{BR}(D^{*+} \to D^+\pi^0)$ from the fully reconstructed data and the feeddown peak. The average of these two ratios and the combined result using converted photons is

$$R_+ = -0.02 \pm 0.09 \pm 0.05\,.$$

To extract branching fractions from these measurements, we use two methods: Since the channels $D^{*+} \to D^0\pi^+$ and $D^{*+} \to D^+\pi^0$ are related by isospin and the P-wave factor p^3, one may calculate their ratio from the well known mass differences [8.13] to be

$$\frac{\mathrm{BR}(D^{*+} \to D^0\pi^+)}{\mathrm{BR}(D^{*+} \to D^+\pi^0)} = 2.21 \pm 0.07$$

From this and our best estimate of R_+ the branching fractions are determined to be

$$\mathrm{BR}(D^{*+} \to D^+\pi^0) = (31.2 \pm 1.1 \pm 0.8)\%$$
$$\mathrm{BR}(D^{*+} \to D^0\pi^+) = (68.8 \pm 2.4 \pm 1.3)\%$$
$$\mathrm{BR}(D^{*+} \to D^+\gamma) = (0.0 \pm 2.8 \pm 1.6)\% < 5.2\%\ (90\%\mathrm{CL})$$

The latter result is compared with other experiments in table 4.

Table 4 Results on $\mathrm{BR}(D^{*+} \to \gamma D^+)$.

experiment	BR [%]	0 5 10 20 30 %
Mark I [6]	8 ± 7	
Mark II 82 [3]	22 ± 12	
Mark III 88 [7]	$17 \pm 5 \pm 5$	
CLEO 92 [10]	$1.1 \pm 1.4 \pm 1.6$	
this experiment	< 5.2 (90%CL)	

Alternatively, we calculate the scaled cross section times branching fraction

$$s \cdot \bar{\sigma}(D^{*+}, x_p > 0.65) \cdot \mathrm{BR}(D^{*+} \to D^+\pi^0) \cdot \mathrm{BR}(D^+ \to K^-\pi^+\pi^+) = \frac{N(D^{*+} \to (K^-\pi^+\pi^+)\pi^0)}{\eta \sum L_i/s_i} = (0.805 \pm 0.080 \pm 0.047)\,\mathrm{pb\,GeV^2}$$

and compare it to our previous result [14]

$$s \cdot \sigma(D^{*+}, x_p > 0.65) \cdot \mathrm{BR}(D^{*+} \to D^0\pi^+) \cdot \mathrm{BR}(D^0 \to K^-\pi^+) = (0.796 \pm 0.039 \pm 0.037)\,\mathrm{pb\,GeV^2}$$

In the ratio, the luminosities L_i are almost the same, and do not contribute to the error. The acceptance corrected number $N(D^{*+} \to (K^-\pi^+\pi^+)\pi^0)/\eta = 3502 \pm 350 \pm 205$ has been taken from the fit to the feeddown peak. The second, systematic error is dominated by uncertainties in the acceptance η, and has been obtained using different cuts on the minimum photon energy. Thus we determine

$$\frac{\mathrm{BR}(D^{*+} \to D^0\pi^+)}{\mathrm{BR}(D^{*+} \to D^+\pi^0)} = 2.17 \pm 0.24 \pm 0.16 \pm 0.25$$

where the second error contains the uncertainty in the acceptance, and the third error comes from the uncertainty in the branching fractions of D^0 and D^+. From this, we obtain all branching fractions without any assumption to be

$$\mathrm{BR}(D^{*+} \to D^+\pi^0) = (31.5 \pm 2.7 \pm 3.0)\%$$
$$\mathrm{BR}(D^{*+} \to D^0\pi^+) = (68.5 \pm 3.4 \pm 3.2)\%$$
$$\mathrm{BR}(D^{*+} \to D^+\gamma) = (0.0 \pm 2.9 \pm 1.6)\% < 5.4\%(90\%\,\mathrm{CL})$$

Both results support the recent CLEO measurement, and are in disagreement with the previous large branching fraction for $D^{*+} \to D^+\gamma$.

Acknowledgements

It is a pleasure to thank U. Djuanda, E. Konrad, E. Michel, and W. Reinsch for their competent technical help in running the experiment and processing the data. We thank Dr. H. Nesemann, B. Sarau, and the DORIS group for the operation of the storage ring. The visiting groups wish to thank the DESY directorate for the kind hospitality extended to them.

References

[1] S. Ono, Phys. Rev. Lett. **37**, 655 (1976).
[2] G. Goldhaber et al. (Mark I), Phys. Lett. **69B**, 503 (1977).
[3] M. W. Coles et al. (Mark II), Phys. Rev. **D26**, 2190 (1982).
[4] W. Bartel et al. (JADE), Phys. Lett. **161B**, 197 (1985).
[5] E. H. Low et al. (HRS), Phys. Lett. **B183**, 232 (1987).
[6] C. Simopoulos (Mark III), in Proc. of Int. Symp. on Prod. and Decay of Heavy Flavors, Stanford 1987, ed. E. Bloom, A. Fridman, p. 413.
[7] J. Adler et al. (Mark III), Phys. Lett. **B208**, 152 (1988).
[8] The Particle Data Group, Phys. Rev. **D45**, S1 (1992).
[9] L. Angelos, G. P. Lepage, Phys. Rev. **D45**, 3021 (1992).
[10] F. Butler et al. (CLEO), Phys. Rev. Lett. **69**, 2041 (1992).
[11] H. Albrecht et al., Nucl. Instr. and Meth. **A275**, 1 (1989).
[12] T. Sjöstrand, Comp. Phys. Comm. **27**, 243 (1982). **28**, 229 (1983) and **39**, 347 (1986).
[13] D. Bortoletto et al. (CLEO), Phys. Rev. Lett. **69**, 2046 (1992).
[14] H. Albrecht et al. (ARGUS), Z. Phys. **C52**, 353 (1991).

Figures

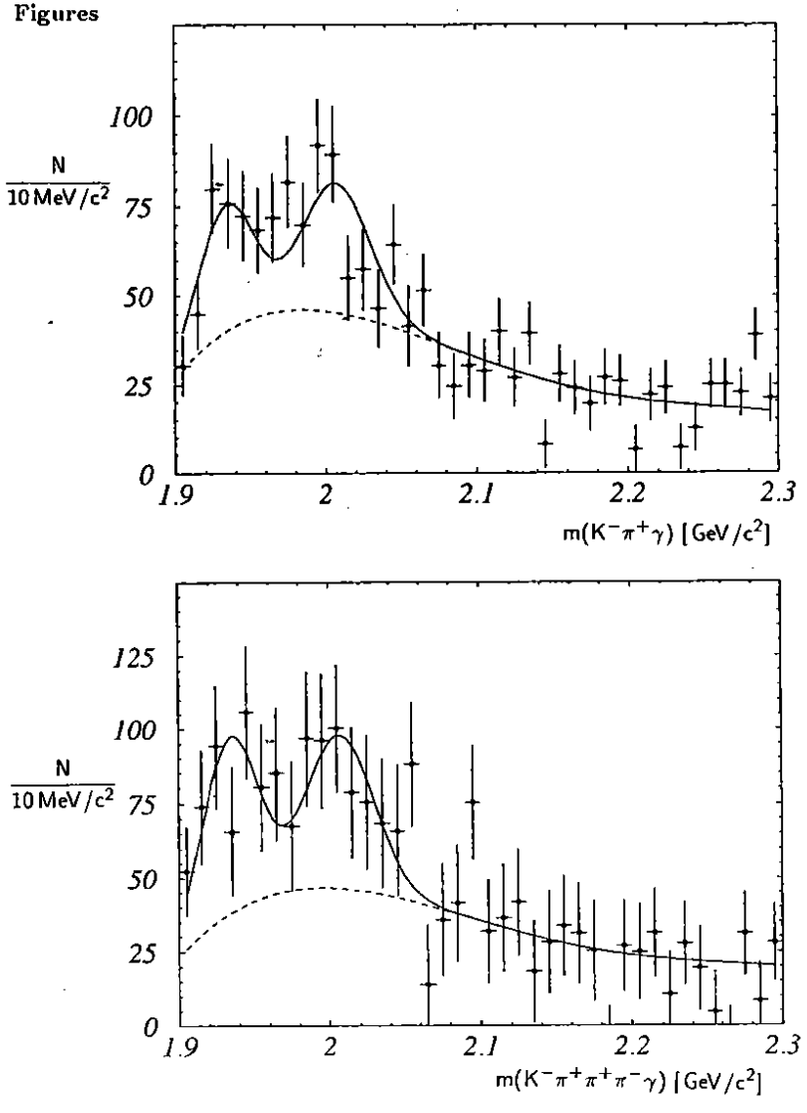

Fig. 1 Invariant mass distribution of $D^{*0} \to D^0\gamma$ candidates. The upper plot shows the $D^0 \to K^-\pi^+$ candidates, the lower plot the $K^-\pi^+\pi^+\pi^-$ channel. The solid line is the result of the fit described in the text, the dashed line shows the background distribution.

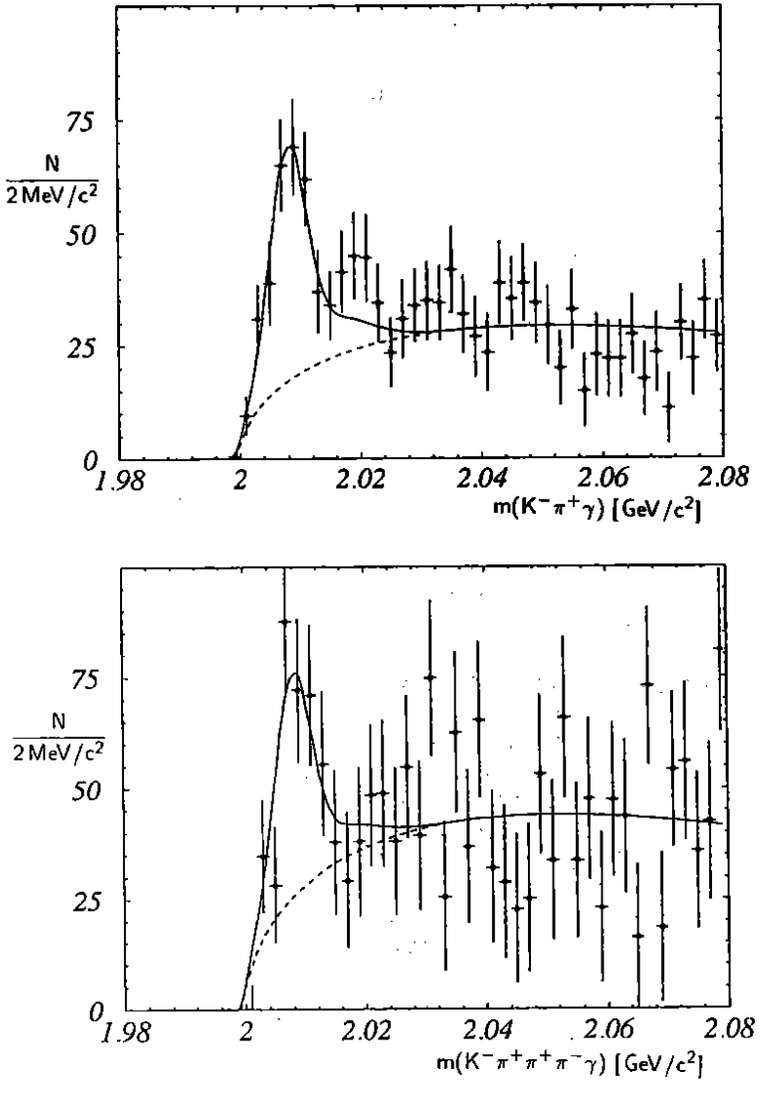

Fig. 2 Invariant mass distribution of $D^{*0} \to D^0\pi^0$ candidates. The upper plot shows the $D^0 \to K^-\pi^+$ candidates, the lower plot the $K^-\pi^+\pi^+\pi^-$ channel. The solid line is the result of the fit described in the text, the dashed line shows the background distribution.

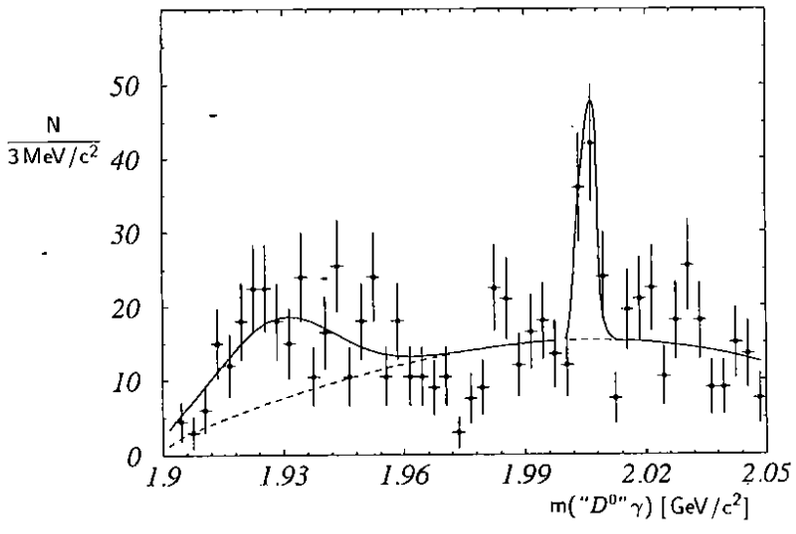

Fig. 3 Invariant mass distribution of $D^{*0} \rightarrow D^0\gamma$ candidates with converted photons. The solid line is the result of the fit described in the text. The dashed line shows the background distribution.

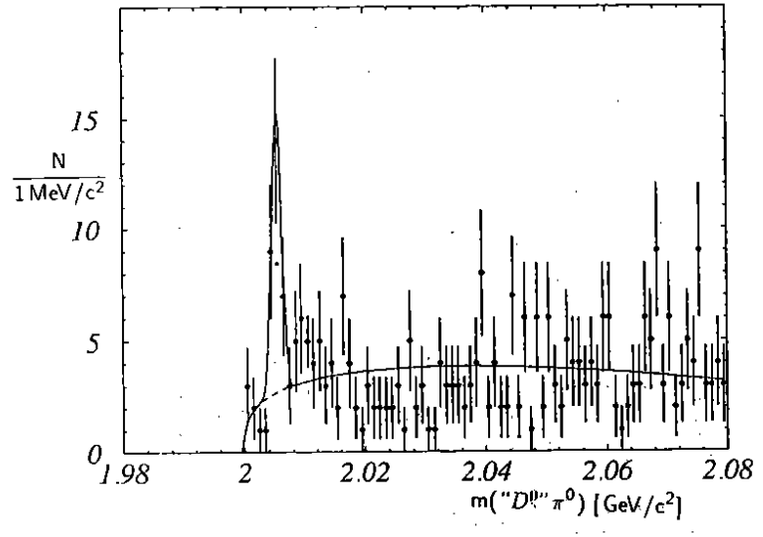

Fig. 4 Invariant mass distribution of $D^{*0} \rightarrow D^0\pi^0$ candidates, with $\pi^0 \rightarrow \gamma_c\gamma$. The solid line is the result of the fit described in the text, the dashed line shows the background distribution.

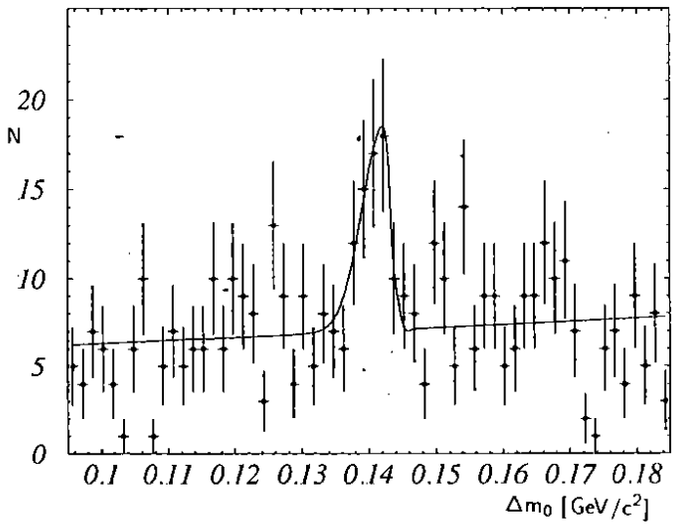

Fig. 5 Mass difference $\Delta m_0 = m(D^{*0}) - m(D^0)$ of $D^{*0} \to D^0\pi^0$ and $D^{*0} \to D^0\gamma$ candidates, using both D^0 decay channels, and converted photons.

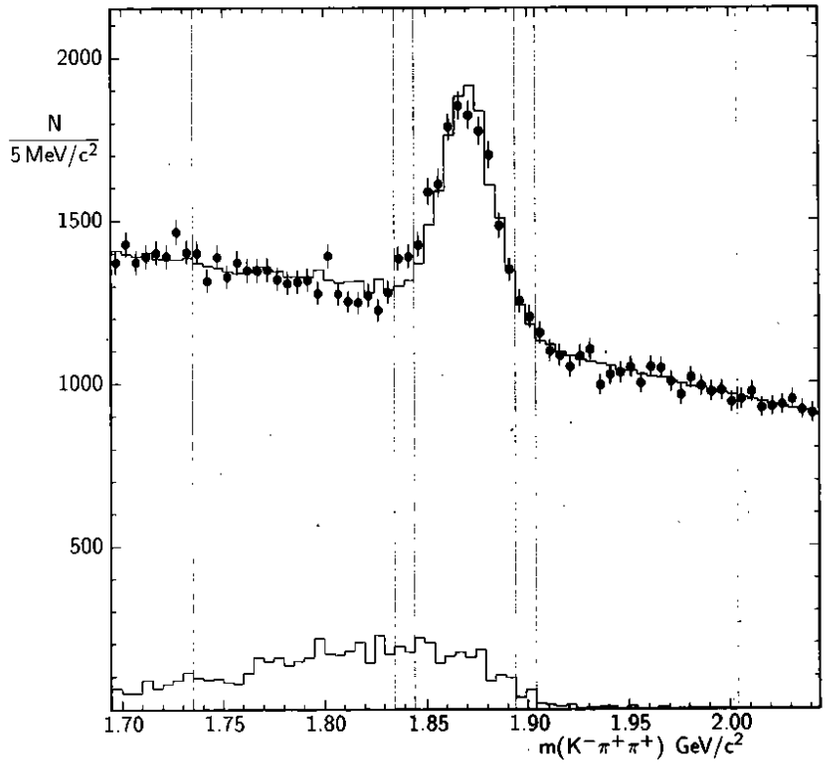

Fig. 6 Invariant mass distribution of $K^-\pi^+\pi^+$ combinations. with limits of the signal and sideband regions. The points are data. the histogram is the result of the fit described in the text. The lower histogram shows the shape of misidentified $D_s \to K^-K^+\pi^+$ decays.

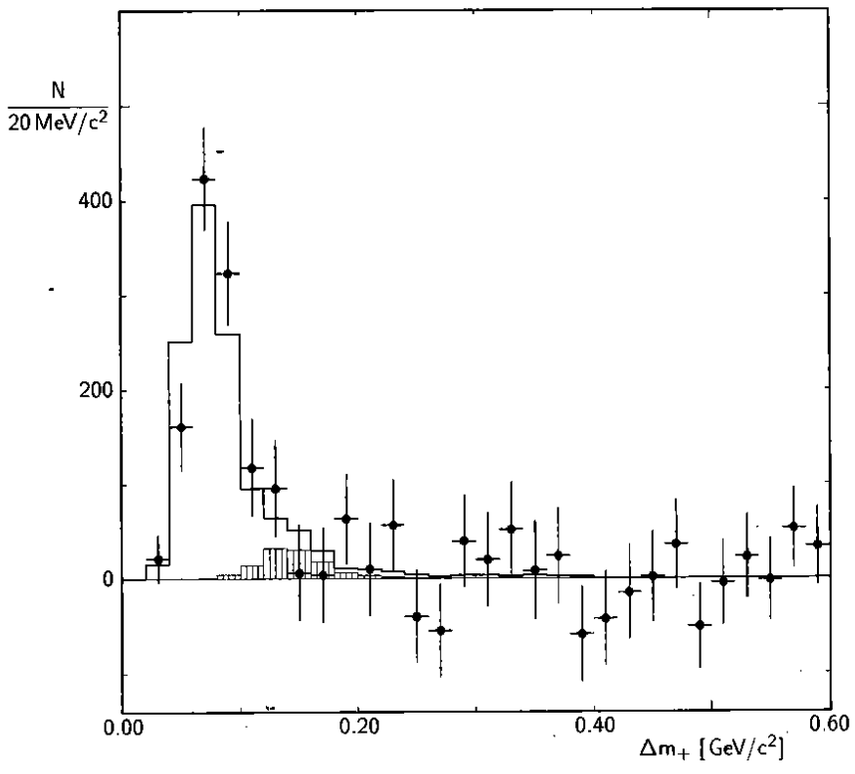

Fig. 7 Distribution of the mass difference $\Delta m_+ = m(D^{*+}) - m(D^+)$ for $D^{*+} \to D^+\gamma$ candidates, after subtraction of all random combinations. The solid histogram is the result of the fit described in the text, showing a prominent peak from the $D^{*+} \to D^+\pi^0 \to D^+\gamma(\gamma)$ decay. The hatched histogram represents the $D^{*+} \to D^+\gamma$ and $D_s^* \to D_s\gamma$ part, and is completely saturated by the expectation for the latter decay.

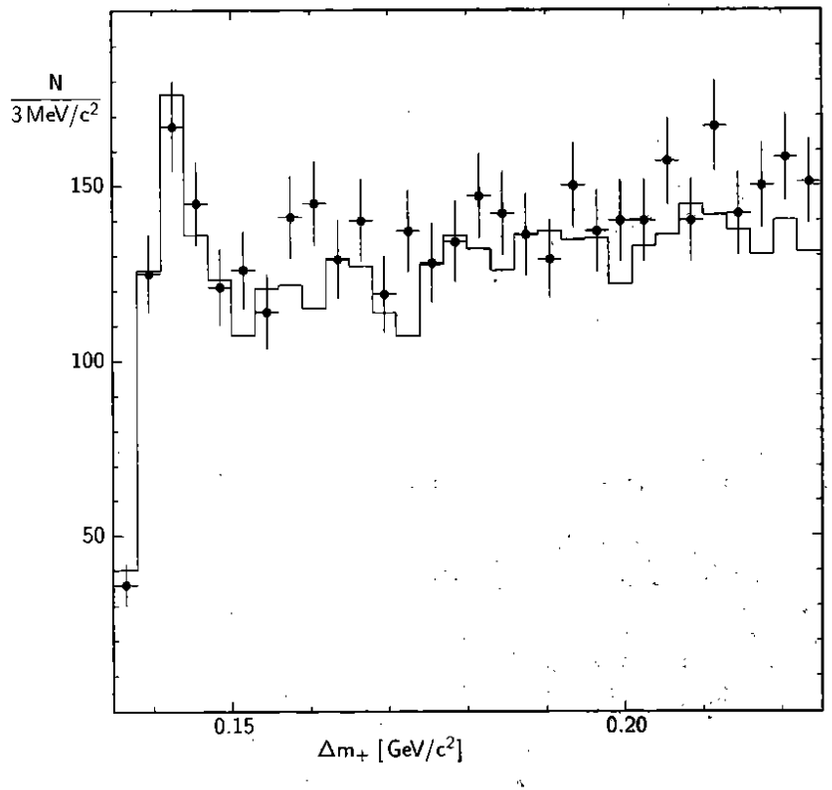

Fig. 8 Mass difference distribution of $D^{*+} \to D^+\pi^0$ candidates. The solid histogram is the sum of all combinatoric backgrounds, plus a fitted signal peak with a shape defined by the Monte Carlo simulation.

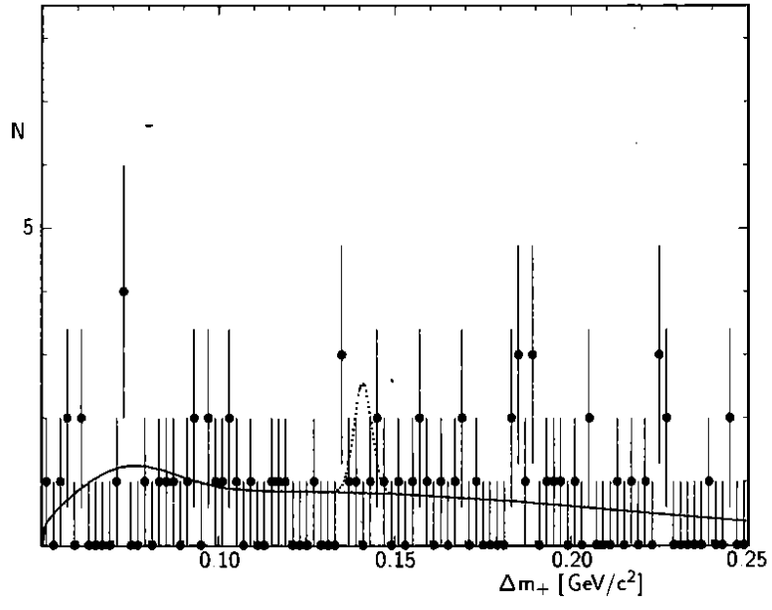

Fig. 9 Invariant mass difference distribution of $D^{*+} \rightarrow D^+\gamma$ candidates with converted photons. The solid line is the result of the fit described in the text. The dotted line shows the upper limit for a $D^+\gamma$ signal at 90%CL.

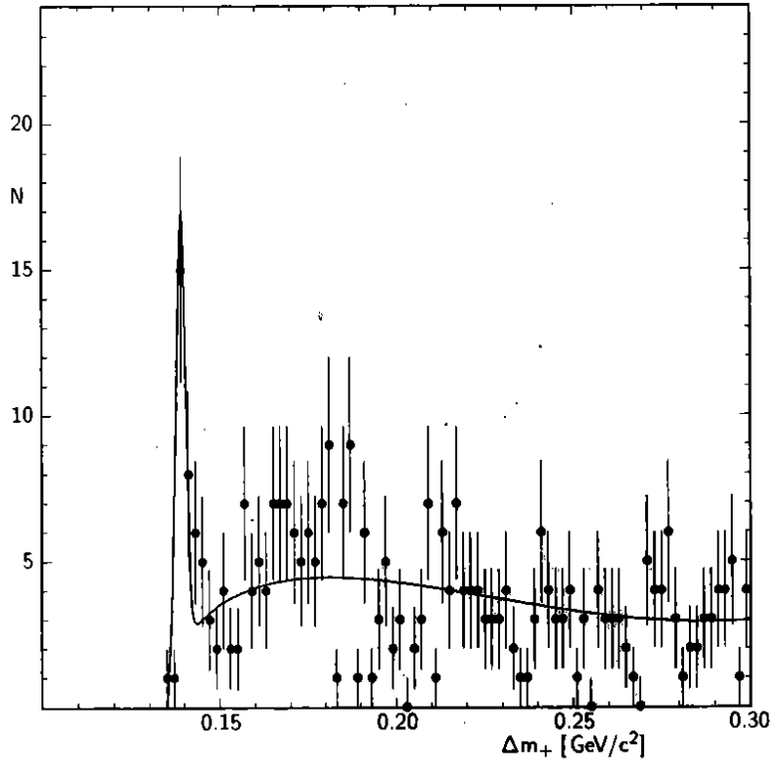

Fig. 10 Invariant mass difference distribution of $D^{*+} \rightarrow D^+\pi^0$ candidates, with $\pi^0 \rightarrow \gamma_c\gamma$. The solid line is the result of the fit described in the text.